Steel and Composite Structures, *Vol. 21, No. 4 (2016) 949-962*
DOI: http://dx.doi.org/10.12989/scs.2016.21.4.949

Analysis of large deformation and fatigue life of fabric braided composite hose subjected to cyclic loading

J.R. Cho [*1] and Y.H. Kim [2]

[1] *Department of Naval Architecture and Ocean Engineering, Hongik University, Sejong 339-701, Korea*
[2] *School of Mechanical Engineering, Pusan National University, Pusan 609-735, Korea*

(*Received March 22, 2016, Revised June 24, 2016, Accepted June 28, 2016*)

Abstract. The braking hose in the automotive hydraulic braking system exhibits the complicated anisotropic large deformation while its movable end is moving along the cyclic path according to the steering and bump/rebound motions of vehicle. The complicated large deformation may cause not only the interference with other adjacent automotive parts but also the durability problem resulting in the fatal microcraking. In this regard, the design of high-durable braking hose with the interference-free layout becomes a hot issue in the automotive industry. However, since it has been traditionally relied on the cost-/time-consuming trial and error experiments, the cost- and time-effective optimum design method that can replace the experiment is highly desirable. Meanwhile, the hose deformed configuration and fatigue life are different for different hose cyclic paths, so that their characteristic investigation becomes an important preliminary research subject. As a preliminary step for developing the optimum design methodology, we in this study investigate the hose deformed configuration and the fatigue life for four representative hose cyclic paths.

Keywords: fabric braided composite hose; cyclic path; anisotropic large deformation; in-plane and out-of-plane; fatigue life

1. Introduction

Braking hose in the automotive hydraulic braking system plays an important role of delivering the driver's braking force to the brake disc cylinders via internal working oil. Since the traffic accidents caused by the oil leakage may lead to the fatal casualties, the braking hose should be elaborately designed to prevent the microcraking (Kwack and Choi 2009), a main source of oil leakage, within the whole period of its warranty. The microcraking is mostly attributed to the complicated and cyclic large deformation of hose and to the interference with other adjacent vehicle components. For this reason, the braking hose is in the lamination composition of pure rubber layers and fabric braided layers to effectively prevent the oil leakage and to suppress the excessive large deformation (Entwistle 1981, Cho *et al*. 2013). The fabric braided layers are composed of periodic warp and fill tows in the complex pattern, so those exhibit the anisotropic behavior even though their base materials are isotropic material (Cho *et al*. 2006, Xu *et al*. 2012, Chuda-Kowalska and Garstecki 2016). Because of the anisotropic behavior of fabric braided layers,

*Corresponding author, Associate Professor, E-mail: jrcho@hongik.ac.kr

http://www.techno-press.org/?journal=scs&subpage=6 ISSN: 1229-9367 (Print), 1598-6233 (Online)

the whole braking hose exhibits the inherent out-of-plane deformation during the steering and bump/rebound motions of vehicle (Cho *et al*. 2013). And, it becomes one of crucial factors in the design of oil leakage-proof high-durable braking hose, which produces the interference-free deformed configuration, by utilizing the computer-aided simulation.

According to the worldwide intensification on the durability regulation of key automotive parts (Mayyas *et al*. 2012), the hose configuration prediction and the durability assurance become a hot issue in the automotive industry. To accomplish this goal, several core subjects such as the elaborate material modeling of the fabric braided layer, the identification and interpolation of hose cyclic paths and the characteristic investigation of deformed configuration and critical fatigue life should be fully considered. The hose cyclic path is not unique but manifold depending on the combination of the steering and bump/rebound motions of vehicle (Cho *et al*. 2015). So, a number of major cyclic paths that characterize the hose deformed layout should be identified and numerically interpolated for the numerical simulation. Meanwhile, for the large deformation analysis for the specific hose cyclic path, one may try to simplify the braided layer as an isotropic material because its solid modeling by considering the detailed geometry is painstaking and impractical (D'Amato 2001, Sun *et al*. 2003, Cho *et al*. 2006, Zhang and Xu 2013). However, this simple model, which is applicable only to the extremely simple loading conditions like the pure extension, cannot successfully represent the out-of-deformation. Hence, the reliability of deformed configuration and fatigue life that are numerically predicted using the simple hose model is highly questionable.

For this reason, the hose deformed configuration path and the resulting fatigue life have been traditionally evaluated by experiments. However, this approach is highly cost- and time-consuming, and furthermore it leads to the hose layout design of trial and error. To overcome the demerits of experimental approach, the attempts to apply the analytical and computational methods have been attempted by several investigators. Sugiyama and Otaki (1992) analytically predicted the hose deformed shape using a mathematical model that is constructed with the beam elements and particles and compared with the experiment. Keil *et al*. (2002) simulated the movement of braking hose by utilizing the CAD system and compared the hose deflection using ADAMS that is commercial software for the multibody dynamics simulation. Cho *et al*. (2013, 2015) introduced a homogenization approach for modeling the fabric braided layers as the homogenized orthotropic layers and applied to the large deformation and fatigue analyses using 3-D nonlinear finite element method.

As an extension of our previous work (Cho *et al*. 2013, 2015) on the braking hose, this paper intends to investigate the characteristics of hose large deformation and fatigue life to the hose cyclic path. The ultimate goal of our research is to develop an optimization method for designing the high-durable braking hose and its optimum layout, and the current study is a preliminary stage for our ultimate goal. The four representative cyclic paths are chosen, and the large deformation and fatigue analyses are carried out for each cyclic path. The previous homogenization, path interpolation and fatigue evaluation methods are integrated, and the variation of the maximum in-plane and out-of-plane deformations and the critical fatigue life cycles are comparatively investigated to the hose cyclic path.

2. Braking hose in large deformation cyclic motion

Fig. 1(a) represents a typical braking hose assembled in the front braking system, where one end is fixed to the main body of vehicle while the other end, called the movable end throughout

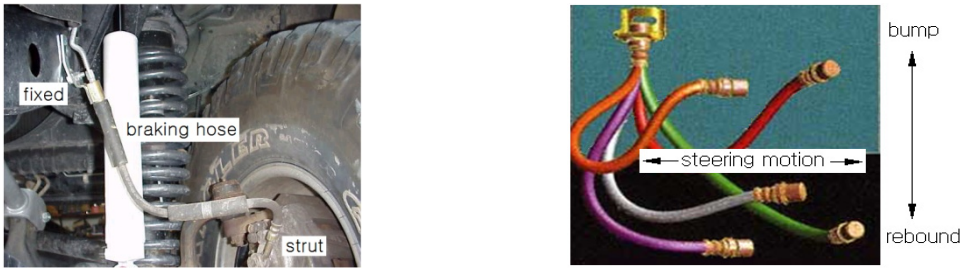

(a) (b)

Fig. 1 (a) Braking hose assembled in the front wheel; (b) steering and bump/rebound motions

this manuscript, is attached to the tire assembly using a strut. Hence, the hose movable end is to be moved along with the tire motion, and hence the entire braking hose is forced to be deformed. As shown in Fig. 1(b), the vehicle motion could be classified into the horizontal steering mode and the vertical bump/rebound mode. Here, the bump/rebound motion is resulted from the relative vertical movement of tire with respect to the vehicle at quick stop or start, or when the vehicle is running over cleats. For a given braking hose, its deformation is not unique but diverse in aspects of the deformed configuration and the deformation magnitude, depending on the moving path of hose movable end. The hose deformation is not only large and complicated but also repetitive, so that the deformed braking hose may contact with other adjacent automotive parts and the hose durability deteriorates in proportional to the repetition number of cyclic deformations.

2.1 Cyclic paths and their numerical interpolation

The path of hose movable end is not easy to identify because it is diversely determined according to a combination of the tire steering motion and the bump/rebound motion of vehicle. In fact, its realistic and exact identification would be possible only by either the motion measurement using the vision system or 3-D multibody dynamics (MBD) simulation. However, even if possible, such measurement or MBD simulation requires the painstaking job for processing the numerous motion data. For this reason, the path is rather simply defined using nine extreme positions shown in Fig. 2(a) that are determined by the tensor product of three positions in the steering mode and three positions in the bump/rebound mode. The neutral position corresponds to the straight driving

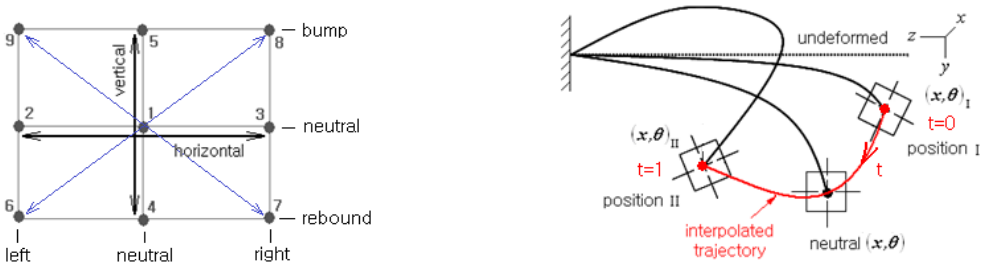

(a) (b)

Fig. 2 Paths of hose movable end: (a) nine extreme positions; (b) numerical interpolation

without bump and rebound, and the left and right positions indicate the maximum steering in the left and right directions. Meanwhile, the bump and rebound indicate the maximum compression and stretching of tire in the vertical direction with respect to the vehicle. Referring to Stalnaker and Turner (2002) and Cho *et al*. (2011), the driving conditions are divided into nine modes and those are identical with the above-mentioned nine extreme positions. A number of paths could be defined by choosing three among nine extreme positions, but the validity and importance of defined paths should be examined based on the real driving conditions of vehicle. Two most representatives are the horizontal path 2-1-3 and the vertical 4-1-5, where the former corresponds to the left-neutral-right handling in cruising while the latter to the center acceleration and braking, respectively. And, their cyclic paths are defined as follows: for example, 1-2-1-3-1 for the horizontal and 1-4-1-5-1 for the vertical.

The identification of nine extreme positions is much simpler and easier than that for the whole path, and it is made by measuring three translation co-ordinates $\{x(t), y(t), z(t)\}$ and three rotation angles $\{\theta_x(t), \theta_y(t), \theta_z(t)\}$ of the strut (i.e., the hose movable end) with respect to the fixed co-ordinate system positioned at any reference point on the frame of vehicle. Once a path is identified in terms of three extreme positions, its whole path (or, trajectory) could be approximated by the numerical interpolation method. For the sake of explanation, let us consider the path containing the neutral position, as illustrated in Fig. 2(b). Six co-ordinates of the hose movable end on the path are interpolated using second-order polynomials, and the corresponding coefficients a_{ij} and b_{ij} are determined by solving the following two linear equation systems given by

$$\begin{Bmatrix} x(t) \\ y(t) \\ z(t) \end{Bmatrix} = \begin{bmatrix} a_{11} & a_{12} & a_{13} \\ a_{21} & a_{22} & a_{23} \\ a_{31} & a_{32} & a_{33} \end{bmatrix} \begin{Bmatrix} 1 \\ t \\ t^2 \end{Bmatrix}, \quad \begin{Bmatrix} \theta_x(t) \\ \theta_t(t) \\ \theta_z(t) \end{Bmatrix} = \begin{bmatrix} b_{11} & b_{12} & b_{13} \\ b_{21} & b_{22} & b_{23} \\ b_{31} & b_{32} & b_{33} \end{bmatrix} \begin{Bmatrix} 1 \\ t \\ t^2 \end{Bmatrix} \tag{1}$$

with the known values at three extreme positions and the parameter $t \in [0, 1]$. Here, the values of parameter t at the neutral position for each co-ordinate are calculated by

$$t_{neutral} = \frac{|A_{neutral} - A_I|}{|A_{II} - A_I|}, \quad A = x, y, \cdots, \theta_z \tag{2}$$

where the subscripts *neutral*, *I* and *II* are used to indicate six co-ordinates at positions I, II and neutral shown in Fig. 2(b). The interpolated co-ordinates are used as the displacement boundary condition that should be specified to the hose movable end for the incremental large deformation analysis.

2.2 Micro modeling and homogenization of fabric braid

Fig. 3(a) shows a five-layered reinforced braking hose composed of three rubber layers and two fabric braided layers, where the layers are assumed to be perfectly bonded. The unfold configuration of braided layer is represented in Fig. 3(b), where warp and fill tows are woven with the specific helix angle α_H. Each warp and fill tow are composed of three polyester cords, and the interfaces between warp and fill tows are also assumed to be perfectly bonded. The total number of bundles (i.e., warp and fill tows) within a pitch p is defined by *Cr* and the diameter of base cord is denoted by *denia* which is defined by the total weight in gram per 9,000 m of cord. These material

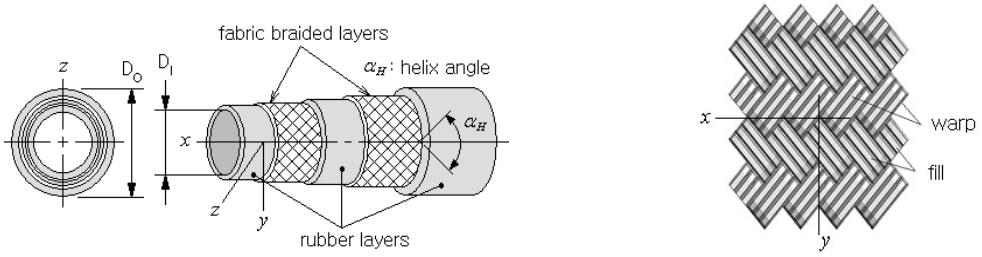

(a) (b)

Fig. 3 Fabric braided rubber hose: (a) layer composition; (b) unfolded fabric braid

parameters as well as the helix angle, that are usually different for the inner and outer braided layers, are key parameters influencing the anisotropic behavior of braided layer.

The microstructure of fabric braided layer is to be reoriented (Ivanov and Tabiel 2002) with the negligible strain during the deformation of braking hose up to the critical strain value. The reorientation causes the change of helix angle, which in turn results in the change of effective mechanical properties of fabric braid. The reorientation phenomenon is a highly nonlinear problem because the change of helix angle cannot be found until the numerical simulation is completed. In fact, the strains of fabric braided layers are much smaller than those of rubber layers, so this phenomenon is ignored for the current study and the anisotropic behavior is modeled as a small-strain homogenized orthotropic solid, that is, the St. Venant-Kirchhoff model. With the setting of material co-ordinates shown in Fig. 3, two fabric braided layers are modeled as an orthotropic material with the constitutive relation (Daniel and Ishai 1994) given by

$$\begin{Bmatrix} \sigma_1 \\ \sigma_2 \\ \sigma_3 \\ \tau_{23} \\ \tau_{31} \\ \tau_{12} \end{Bmatrix} = \begin{bmatrix} D_{11} & D_{12} & D_{13} & 0 & 0 & 0 \\ D_{21} & D_{22} & D_{23} & 0 & 0 & 0 \\ D_{31} & D_{32} & D_{33} & 0 & 0 & 0 \\ 0 & 0 & 0 & D_{44} & 0 & 0 \\ 0 & 0 & 0 & 0 & D_{55} & 0 \\ 0 & 0 & 0 & 0 & 0 & D_{66} \end{bmatrix} \begin{Bmatrix} \varepsilon_1 \\ \varepsilon_2 \\ \varepsilon_3 \\ \gamma_{23} \\ \gamma_{31} \\ \gamma_{12} \end{Bmatrix} \tag{3}$$

with six diagonal terms defined by $D_{ij} = (1 - \nu_{jk}\nu_{kj})/E_jE_k\Delta$ and $D_{i+3i+3} = G_{ij}$. The other six off-diagonal terms are defined by

$$D_{ij} = \frac{\nu_{ji} + \nu_{ki}\nu_{jk}}{E_jE_k} \quad (i \to j \to k), \quad D_{kj} = \frac{\nu_{jk} + \nu_{ik}\nu_{ji}}{E_iE_j} \quad (k \to j \to i) \tag{4}$$

with $\Delta = (1 - \nu_{12}\nu_{21} - \nu_{23}\nu_{32} - \nu_{31}\nu_{13} - 2\nu_{12}\nu_{23}\nu_{31})/E_1E_2E_3$. Where, subscripts 1, 2 and 3 stand for x,y and z, respectively.

Meanwhile, the incompressible hyperelastic behavior of three rubber layers is modeled by a four-term Mooney-Rivlin material model which is expressed by the strain energy density functional $W(I_1, I_3, I_3)$ defined by

$$W(I_1, I_2, I_3) = C_{10}(I_1 - 3) + C_{01}(I_2 - 3) + C_{20}(I_1 - 3)(I_2 - 3) + \frac{\kappa}{2}(I_3 - 1)^2 \quad (5)$$

In which, I_i are the invariants of Green-Lagrange strain tensor and C_{ij} are the material dependent Mooney-Rivlin constants. The incompressibility of rubber is enforced by the last term on the right hand side of Eq. (5), where the incompressibility enforcement becomes higher in proportional to the value of parameter κ. The Mooney-Rivlin constants which were determined by the uniaxial tension test of rubber specimen are given in Table A1 in Appendix.

3. Deformed configuration and durability of braking hose

3.1 Geometric interpretation of hose deformed configuration

The layout design of braking hose based on the deformed configuration is an important subject because the sliding contact of the braking hose with other adjacent vehicle parts wears down the outer rubber layer. The continuation of such wearing down not only weakens the structural strength of hose but also causes the fatal oil leakage. However, the layout design has been traditionally performed based on the trial and error experiments because the complex anisotropic hose deformation cannot be accurately analyzed by the conventional simple isotropic hose model as mentioned earlier. In fact, the layout design is a troublesome task because the hose deformed configuration is path-dependent and continuously varying with the hose movement. In other words, the designer should evaluate a huge amount of deformation data at every moving stage on various hose paths, in order to extract the characteristic deformation magnitude that will be used for the layout design.

In this regard, the numerical approach employing an appropriate anisotropic hose model can successfully resolve the above-mentioned problems of the traditional experiment-based layout design, because it can accurately and quickly obtain and evaluate the hose deformation data for various hose paths. Meanwhile, the choice of characteristic deformation magnitude depends on the design standards of car maker, but we in this study choose two principal maximum deformations to investigate the deformation configuration to the hose path. Referring to Fig. 4, one is the maximum in-plane deformation and the other is the maximum out-of-plane deformation, and the both are measured with respect to the straight line $a - a'$ connecting two hose ends. The largest normal distance between the deformed hose and the straight line always becomes the maximum in-plane deformation, while the other on the plane normal to the in plane becomes the maximum out-of-plane deformation.

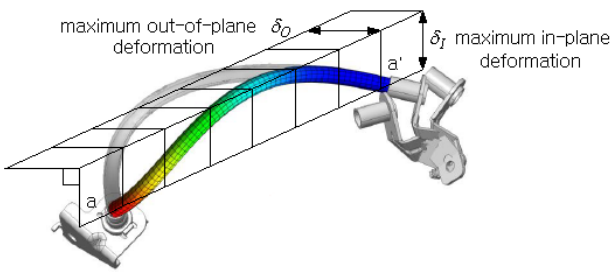

Fig. 4 Maximum in-plane and out-of-plane deformations of braking hose

3.2 Fatigue life evaluation

The cyclic motion of braking hose along a specific path produces the complex cyclic variations of strains and stresses, with the presence of mean strain and stress that are resulted from the pre-deformation caused when the braking hose is assembled at the neutral position. It is known that the mean strain and stress have a significant effect on the fatigue life, such that the tensile mean strain and stress are detrimental while the compressive ones are beneficial. When the applied stresses generate predominantly elastic strain amplitudes, the mean stress effect can be taken into consideration by Basquin's mean stress correction method (Basquin 1910, Karolczuk *et al*. 2013) given by $\sigma_{ar} = \sigma'_f(2N_f)^b$, where N_f is the fatigue life, σ'_f the fatigue strength coefficient, and b the fatigue strength exponent, respectively. Here, σ_{ar} $(=\sqrt{\sigma_{\max}\sigma_a})$ denotes the equivalent fully reversed stress amplitude defined in terms of the maximum stress $\sigma_{\max}$ and the stress amplitude σ_a. But, when the cyclic response of the material is within the elastic-plastic stress-strain range, the mean stress effect on fatigue life is based on the strain-life approach represented by

$$\frac{\Delta\varepsilon}{2} = \varepsilon_a = \frac{\Delta\varepsilon^e}{2} + \frac{\Delta\varepsilon^p}{2} = \frac{\sigma'_f}{E}\left(2N_f\right)^b + \varepsilon'_f\left(2N_f\right)^c \tag{6}$$

where ε_a is the strain amplitude, ε'_f the fatigue ductility coefficient, and c the fatigue ductility exponent, and E the elastic modulus. The modification of Eq. (6) which is used to predict the fatigue life only at zero mean stress was made by several investigators (Smith *et al*. 1970, Ince and Glinka 2011). The current study utilizes the Morrow model given by

$$\frac{\Delta\varepsilon}{2} = \frac{\sigma'_f - \sigma_m}{E}\left(2N_f\right)^b + \varepsilon'_f\left(2N_f\right)^c \tag{7}$$

By the way, this correction model is needed to be slightly modified for the current study because the large deformation analysis of braking hose is carried out using the Moonley-Rivlin hyperelastic material model by neglecting the plastic strain. Furthermore, the term σ'_f / E is replaced with a material-dependent fatigue parameter K_f which can be determined from the $\varepsilon - N$ curves shown in Fig. 5(a) in the log-log scale. Then, we have the modified Morrow model given by

$$\frac{\Delta\varepsilon}{2} = \left(K_f - \varepsilon_m\right)\left(2N_f\right)^b \tag{8}$$

Here, the $\varepsilon - N$ curves shown in Fig. 5(a) were obtained by the specimen fatigue test at Hwaseung R&A (Cho *et al*. 2015), and two fatigue parameters K_f and b in the modified Morrow model in Eq. (8) are found to be: 30.7003 and -0.8754 for the inner rubber layer and 18.1773 and -0.9067 for the outer rubber layer, respectively. The reader may refer to our previous paper (Cho *et al*. 2015) for the derivation of modified SWAT (Smith-Watson-Topper) model (Smith *et al*. 1970) and the comparison of the modified Morrow model with the SWAT and basic models (6). Differing from the Morrow model in which the effect of mean strain is included, the SWAT model considers the effect of mean stress on the fatigue damage.

The fatigue life assessment is performed for each cyclic path, for which the whole trajectory of hose movable end along the path is approximated by quadratically interpolating its 6-DOFs at

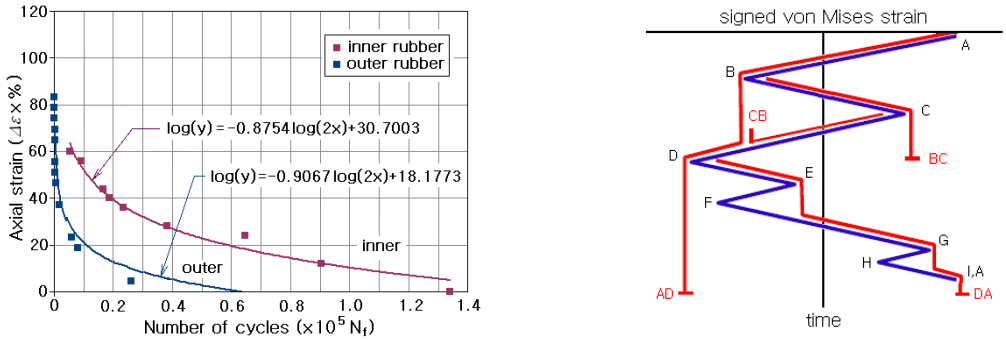

(a) (b)

Fig. 5 (a) The $\varepsilon - N$ curves of two rubber layers; (b) rainflow cycle counting

several discrete locations on the path, as explained in Section 2.1. Since strains and stresses at each material point exhibit the complex time histories composed of a number of harmonic cycles, as illustrated in Fig. 5(b), we employ the Palmgren-Minor cumulative damage law (Palgren 1924) given by

$$D_f = \sum_{i=1}^{N_s} D_i, \quad \left(D_f\right)_i = \frac{n_i}{\left(N_f\right)_i} \tag{9}$$

to calculate the total accumulated fatigue damage D_f along the specific cyclic path. Here, N_s is the total number of distinct harmonic strain cycles, $(D_f)_i$ the accumulated fatigue damage by the i-th harmonic strain cycle, and n_i and $(N_f)_i$ the repetition number and the fatigue life of the i-th strain cycle, respectively. Then, the fatigue life N_f (cycles) at each material point within the braking hose along the specific path is calculated by $N_f = 1 / D_f$. The fatigue life calculation is performed node by node using the signed nodal von Mises strains $\pm \varepsilon_{vm}$ which are recovered using those at Gauss integration points. Here, the signs of von Mises strain (Li and de Freitas 2002) are determined by the sign of the first principal strain ε_1. The repletion numbers n_i of each distinct strain cycle are counted by the rainflow cycle counting method (Rychlik 1987).

4. Numerical experiment

Fig. 6(a) represents a finite element model of five-layered braking hose of the length L of 230 mm and the outer diameter D_o of 10.5 mm. The top end is clamped while the bottom end is forced to move along the predefined path shown in Fig. 2(a), where the center co-ordinates and rotations of the cross-section of the bottom end at nine extreme positions are given in Table 1. Referring to the previous Fig. 3, the thicknesses of five layers are as follows: 1.25, 0.30 and 1,10 mm for the outer, middle and inner rubber layers and 0.45 mm for the outer and inner fabric braided layers. Two fabric braided layers are manufactured with PVA (poly vinyl alcohol) and the helix angles α_H, pitch p and C_r are as follows: 18.5 mm, 24 and 53.64° for the outer layer and 14.0 mm, 20 and 55.57° for the inner layer. The homogenized orthotropic material properties of the inner and outer fabric braided layers are given in Table A2 in Appendix. The reader may refer to our previous paper (Cho *et al*. 2013) for the detailed material properties of PVA cords and the detailed

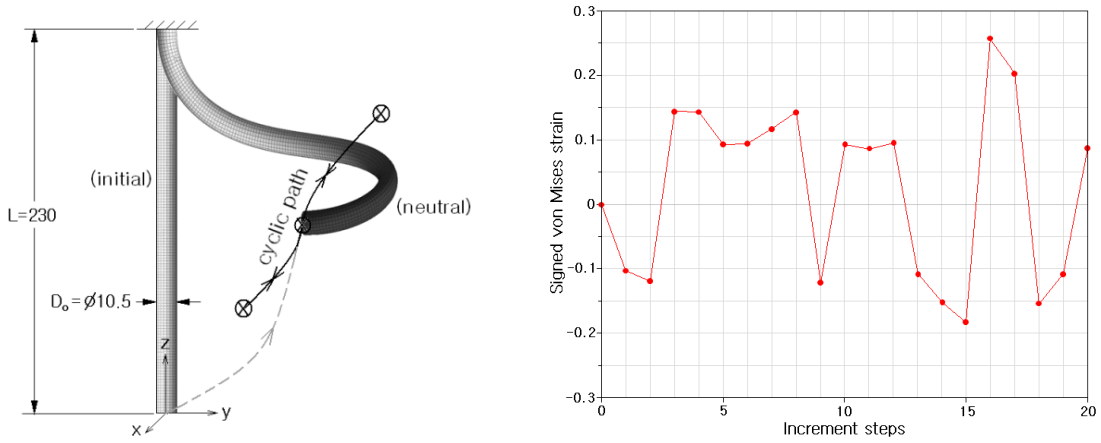

(a) (b)

Fig. 6 (a) Finite element model of braking hose; (b) variation of signed von Mises strain

derivation of homogenized orthotropic material properties by the superposition method and the unit-cell finite element analysis. Fig. 6(b) shows a variation of signed von Mises strain at a specific node of the outer rubber layer that was used for the fatigue life calculation.

Three rubber layers are manufactured with EPDM (ethylene-propylene-diene-monomer), and the materials constants in the four-term Mooney-Rivlin material model in Eq. (5) are given in Table A1 in appendix. The fatigue life is evaluated for the outer and inner rubber layers because both layers are weak to fatigue damage and play an important role in preventing the oil leakage. The entire braking hose is uniformly discretized with the total of 33,002 8-node hexahedron elements, and the layers interfaces are assumed to be completely bonded so that FE meshes of two neighboring layers exactly share common nodes at the layer interfaces. Basically, the updated Lagrangian formulation is used to compute the increments of strain and stress during the hose large deformation along the cyclic paths, and the invariants of Green-Lagrange strain tensor in Mooney-Rivlin models were evaluated in the sense of total Lagrangian.

Table 1 The co-ordinates and rotation angles of the hose section at the right movable end

Positions	Center co-ordinates (mm)			Rotation angles (deg)		
	x	y	z	θ_x	θ_y	θ_z
1	-29.143	181.788	226.513	112.900	6.277	55.898
2	-34.787	152.647	224.121	107.916	-17.090	29.548
3	-37.039	206.245	232.331	112.454	28.343	78.412
4	-29.626	174.877	157.083	111.437	6.610	56.182
5	-29.199	178.584	296.895	113.607	6.350	54.783
6	-37.509	145.511	155.235	106.056	-18.233	29.509
7	-36.444	200.500	162.106	111.094	29.892	78.691
8	-38.129	201.735	302.792	113.293	26.944	76.816
9	-32.451	149.582	294.512	108.860	-15.510	29.077

Figs. 7 and 8 represent the in-plane and out-of-plane deformed configurations of the braking hose for four different paths when their deformations reach the peak values. It is clearly observed that the deformed layouts and the maximum values δ_I and δ_O are quite different for different paths. Referring to Fig. 2(a), paths 3 and 4 are defined by the diagonals paths 9-1-7 and 6-1-8, respectively. It is observed that paths 1 and 3 produce relatively larger in-plane deformations, but conversely, the out-of-plane deformations at both paths are shown to be insignificant. In case of the out-of-plane deformation, it is shown to be remarkable at paths 2 and 4. As given in Table 2, the maximum in-plane and out-of-plane deformations are largest at path 1 and 2, respectively, such that δ_I is 71.59 mm while δ_O is 17.75 mm. This comparative investigation confirms the importance of deformation analysis for the hose layout design to avoid the interference with other adjacent automotive parts.

The maximum in-plane and out-of-plane deformations, the peak equivalent strains and stresses and the critical fatigue lives for four different paths are given in Table 2. It is found that both the peak equivalent strain and stress are remarkable at paths 1 and 3, which is because both paths

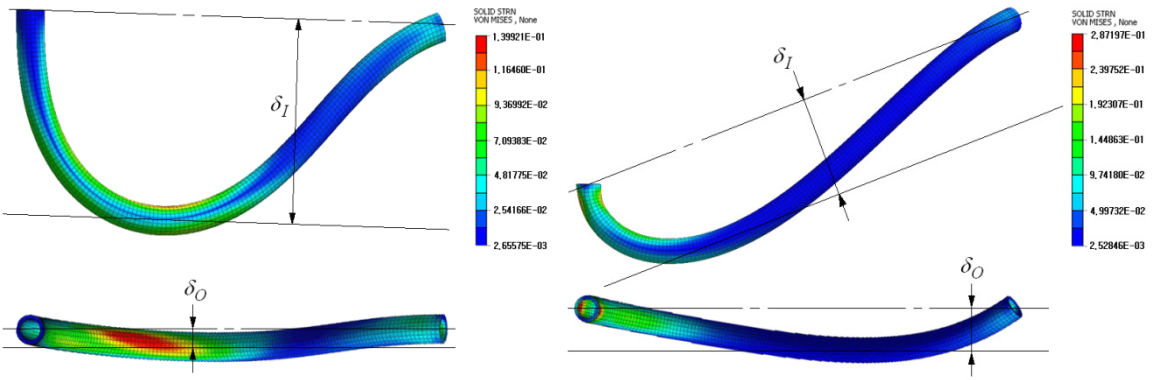

(a) (b)

Fig. 7 Maximum in- and out-of-plane plane deformations: (a) path 1 (horizontal); (b) path 2 (vertical)

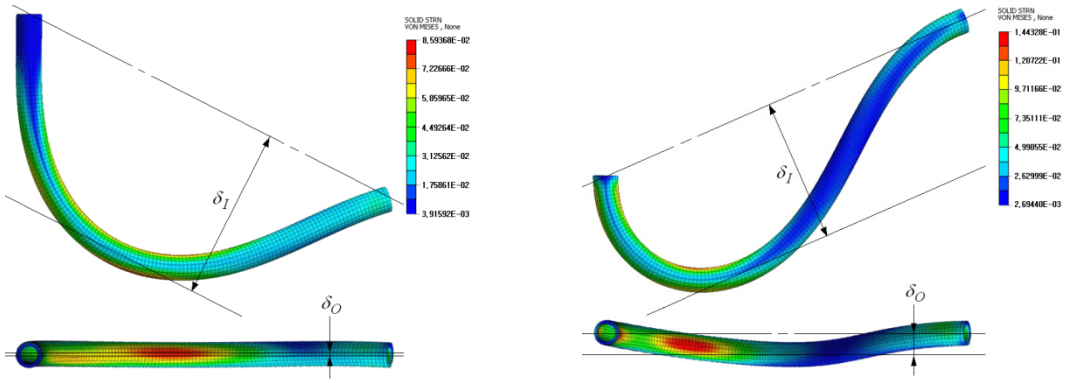

(a) (b)

Fig. 8 Maximum in- and out-of-plane deformations: (a) path 3 (diagonal 1_up-down); (b) path 4 (diagonal 2_down-up)

Table 2 Comparison of the hose deformations, the peak equivalent strains and stresses, and the critical fatigue lives to the cyclic path

Items		Cyclic paths			
		1 (Horizontal)	2 (Vertical)	3 (Diagonal 1)	4 (Diagonal 2)
Maximum deformation (mm)	In-plane	71.59	41.66	70.01	59.52
	Out-of-plane	6.67	17.75	0.95	9.43
Peak equivalent strain		0.582	0.287	0.466	0.144
Peak effective stress (MPa)		4.992	2.485	5.664	1.142
Critical fatigue life (Cycles)	Outer rubber	4,806	21,623	5,735	12,412
	Inner rubber	45,657	133,765	54,482	168,151

produce relatively larger deformations as shown in Figs. 7 and 8. Meanwhile, for all the paths, it is observed that the significantly high strain and stress are produced in the upper one-third region and in the vicinity of lower movable end. It is because the deformation in these regions is characterized by the combined bending and torsion as well as the extension, differing from the intermediate region showing the relatively simple and small deformation. The peak equivalent strain 0.582 is occurred in the vicinity of the upper fixed end at path 1, while the peak effective stress 5.664 MPa appears at the same point but at path 3.

Figs. 9 and 10 comparatively represent the path-wise fatigue life profiles of the outer and inner rubber layers, respectively. First of all, the fatigue lives of inner rubber layers are much higher than those of the outer rubber layer, as given in Table 2, because the magnitude of bending and torsional strain and stress decreases in inverse proportional to the radius of rubber hose. And, all the cases show the remarkably lower fatigue lives in the vicinity of upper fixed and lower movable ends because the equivalent strain is relatively larger in these regions. It implies that the durability of barking hose is determined by these regions, and its improvement could be possible only when the strain level in these regions is reduced. Regarding the hose path, it is found that the critical fatigue

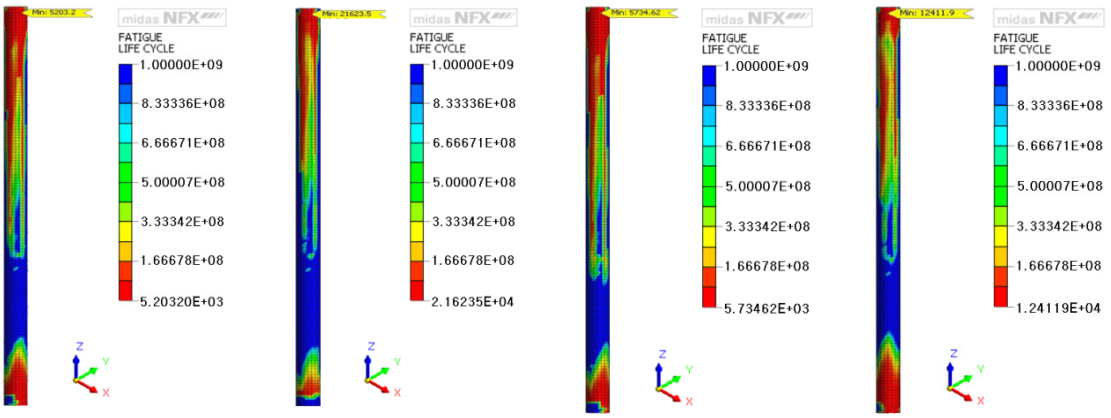

(a) (b) (c) (d)

Fig. 9 Fatigue life profiles of the outer rubber layer: (a) path 1; (b) path 2; (c) path 3; (d) path 4

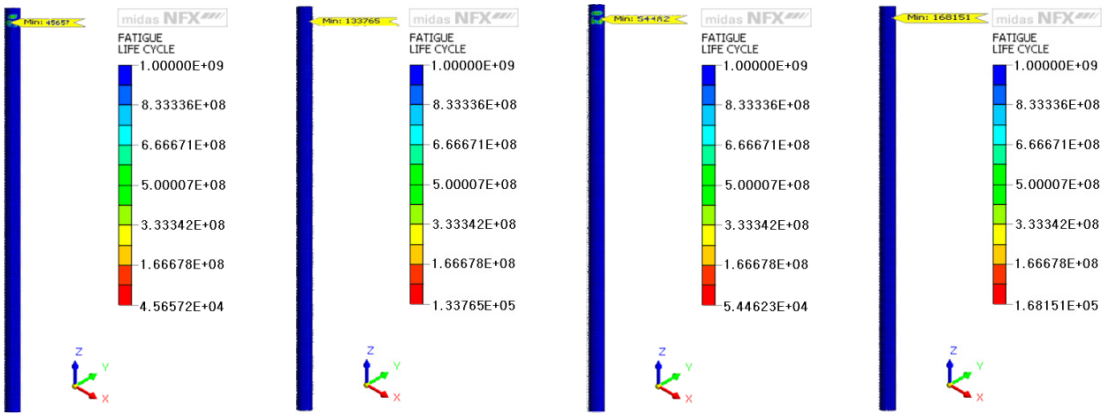

(a) (b) (c) (d)

Fig. 10 Fatigue life profiles of the inner rubber layer: (a) path 1; (b) path 2; (c) path 3; (d) path 4

life is significantly lower at paths 1 and 3 when compared with paths 2 and 4. As given in Table 2, path 1 shows the lowest critical fatigue life equal to 4,806 in the vicinity of upper fixed end. Thus, from the comparative numerical results of the hose deformation and fatigue life, it is found that paths 1 and 3, particularly path 1, should be considered importantly for the layout and durability design of braking hose.

5. Conclusions

As a preliminary step for the layout and durability design of braking hose that exhibits the remarkably complex and anisotropic deformation along the cyclic path, this paper addressed the parametric investigation of hose deformation and fatigue life to four representative hose cyclic paths. Two fabric braided layers were modeled as orthotropic solid ones making use of the unit-cell FE analysis-based homogenization method, and the complicated hose cyclic paths were divided into four representative ones using nine extreme positions of the hose movable ends. The characteristic of hose large deformation was investigated in terms of two principle deformations: the maximum in-plane and out-of-plane deformations, and the fatigue life was evaluated using the modified Morrow fatigue model in which the mean strain is considered. According to our investigation through the numerical experiments, the following main observations are drawn.

(1) The hose deformed configuration depends on the hose path such that the maximum in-plane deformation is prominent at paths 1 (horizontal) and 3 (diagonal 1) but the maximum out-of-plane deformation is remarkable at paths 2 (vertical) and 4 (diagonal 2).
(2) However, all the paths commonly produce larger strain and stress in the upper one-third region and in the vicinity of the lower movable end. This results in the remarkably lower fatigue lives in these regions, particularly at paths 1 and 3.
(3) The outer rubber layer shows much lower fatigue life than the inner rubber layer, and the lowest critical fatigue life equal to 4,806 cycles occurs in the vicinity of upper fixed end at path 1.

And, from the comparative numerical experiment on the hose deformation and fatigue life to

the hose cyclic path, it has been found that paths 1 and 3 are important for the layout and durability design of braking hose.

Acknowledgments

This work was supported by 2016 Hongik University Research Fund. This research was also supported by Basic Science Research Program through the National Research Foundation of Korea (NRF) funded by the Ministry of Education (Grant No. NRF-2014R1A1A2055820).

References

Basquin, O.H. (1910), "The exponential law of endurance tests", *Proc. Am. Soc. Test. Mater.*, **10**(2), 625-630.

Cho, J.R., Song, J.I. and Choi, J.H. (2006), "Prediction of effective mechanical properties of reinforced braid by 3-D finite element analysis", *Key Eng. Mater.*, **306-308**, 799-804.

Cho, J.R., Choi, J.H. and Kim, Y.S. (2011), "Abrasive wear amount estimate for 3D patterned tire utilizing frictional dynamic rolling analysis", *Tribol. Int.*, **44**(7-8), 850-858.

Cho, J.R., Jee, Y.B., Kim, W.J., Han, S.R. and Lee, S.B. (2013), "Homogenization of braided fabric composite for reliable large deformation analysis of reinforced rubber hose", *Composites*: *Part B*, **53**, 112-120.

Cho, J.R., Yoon, Y.H., Seo, C.W. and Kim, Y.G. (2015), "Fatigue life assessment of fabric braided composite rubber hose in compliecated large deformation cyclic motion", *Finite Elem. Anal. Des.*, **100**, 65-76.

Chuda-Kowalska, M. and Garstecki, A. (2016), "Experimental study of anisotropic behavior of PU foam in sandwich panels", *Steel Compos. Struct., Int. J.*, **20**(1), 43-56.

D'Amato, E. (2001), "Finite element modeling of textile composites", *Compos. Struct.*, **54**(4), 467-475.

Daniel, I.M. and Ishai, O. (1994), *Engineering Mechanics of Composite Materials*, Oxford University Press, New York, NY, USA.

Entwistle, K.M. (1981), "The behavior of braided hydraulic hose reinforced with steel wires", *Int. J. Mech. Sci.*, **23**(4), 229-241.

Ince, A. and Glinka, G. (2011), "A modification of Morrow and Smith-Watson-Topper mean stress correction models", *Fatigue Fract. Eng. Mater. Struct.*, **34**(11), 854-867.

Ivanov, I. and Tabiel, A. (2002), "Flexible woven fabric micromechanical material model with fiber reorientation", *Mech. Adv. Mater. Struct.*, **9**(1), 37-51.

Karolczuk, A., Kowalski, M., Banski, R. and Zok, F. (2013), "Fatigue phenomenon in explosively welded steel-titanium clad components subjected to push-pull loading", *Int. J. Fatigue*, **48**, 101-108.

Keil, M., Rodriguez, J. and Hemmye, M. (2002), "Modeling and validation of large hydraulic hose deflections", *SAE Technical Paper*, 2002-01-2589.

Kwack, S.B. and Choi, N.S. (2009), "Micro-damage formation of a rubber hose assembly for automotive hydraylic brakes under a durability test", *Eng. Fail. Anal.*, **16**(4), 1262-1269.

Li, B. and de Freitas, M. (2002), "A procedure for fast evaluation of high-cycle fatigue under multiaxial random loading", *J. Mech. Des.*, **124**(3), 558-563.

Mayyas, A., Qattawi, A., Omar, M. and Shan, D. (2012), "Design for sustainability in automotive industry: A comprehensive review", *Renew. Sustain. Energy Rev.*, **16**(4), 1845-1862.

Palgren, A. (1924), "Die lebensdauer von Kugellagern. Zeitschr VDI", **68**, 339-341.

Rychlik, I. (1987), "A new definition of the rainflow cycle counting method", *Int. J. Fatigue*, **9**(2), 119-121.

Smith, K.N., Watson, P. and Topper, T.H. (1970), "A stress-strain function for the fatigue of materials (Stress-strain function for metal fatigue including mean stress effect)", *J. Mater.*, **5**, 767-778.

Stalnaker, D.O. and Turner, J.L. (2002), "Vehicle and course characterization process for indoor tire wear simulation", *Tire Sci. Technol.*, *TSTCA*, **30**(2), 100-121.
Sugiyama, S. and Otaki, T. (1992), "Mathematical model for brake hose layout", *SAE Technical Paper*, 922123.
Sun, H., Di, S., Zhang, N., Pan, N. and Wu, C. (2003), "Micromechanics of braided composites via multivariable FEM", *Comput. Struct.*, **81**(20), 2021-2027.
Xu, L., Kim, S.J., Ong, C.H. and Ha, S.K. (2012), "Prediction of material properties of biaxial and triaxial braided textile composites", *J. Compos. Mater.*, **46**(18), 2255-2270.
Zhang, C. and Xu, X. (2013), "Finite element analysis of 3D braided composites based on three unit-cell models", *Compos. Struct.*, **98**, 130-142.

CC

Appendix: Material properties of rubber and orthotropic fabric braided layers

Table A1 Mooney-Rivlin constants and bulk modulii of three rubber layers (Cho *et al*. 2015)

Rubber layer	C_{10}	C_{01}	C_{20}	κ
Inner	-1.86902	4.18478	0.41739	1,744.02150
Middle	0.15109	-0.14348	0.38478	7.84270
Outer	-2.46630	4.74565	0.48043	1,225.42264

Table A2 Homogenized orthotropic material properties of two fabric braided layers (Cho *et al*. 2013)

	Young's modulus			Poison's ratio			Shear Modulus		
	E_1	E_2	E_3	v_{12}	v_{23}	v_{31}	G_{12}	G_{23}	G_{31}
Outer	819.2	733.1	1,128.4	0.05	0.16	0.16	14.6	6,490.8	8,241.5
Inner	915.3	801.0	1,547.1	0.03	0.15	0.18	17.8	6,832.7	8,816.2